

Thermal Conductivity Accumulation in Amorphous Materials

Jason M. Larkin¹ and Alan J. H. McGaughey¹

¹*Department of Mechanical Engineering
Carnegie Mellon University
Pittsburgh, PA 15213*

(Dated: August 8, 2013)

By definition, phonons are non-localized propagating vibrations that transport energy over distances much larger than the atomic spacing. For amorphous solids, with the exception of very long-wavelength (low-frequency) modes, the vibrational modes are non-propagating. Recently, experimental measurements of the thermal conductivity of amorphous materials demonstrate that propagating (phonon-like) modes with large mean free paths contribute significantly to thermal transport in amorphous materials.^{1,2} Using broadband frequency domain thermal-reflectance, Regner et al. measured how the thermal conductivity of a-SiO₂ and a-Si thin films change with the penetration depth associated with the heating laser pulse.¹ Regner et al. argue that their measurements probe the mean free paths of propagating vibrational modes to measure the thermal conductivity accumulation function. Using lattice dynamics calculations and molecular dynamics simulations on realistic models of a-SiO₂ and a-Si, we predict and characterize the contributions from propagating and non-propagating vibrations to thermal conductivity. The vibrational mean free paths and (for the first time) the thermal conductivity accumulation functions are predicted for a-SiO₂ and a-Si and compared with experimental results of Regner et al. and varying thin film measurements. For a-SiO₂, the propagating modes are found to contribute negligibly for both bulk and thin films. We demonstrate the scaling of the low-frequency propagating mode diffusivities using (to our knowledge) the largest model of bulk a-Si. For a-Si, the propagating modes contribute significantly to thermal transport. We consider two scalings of the propagating mode diffusivities to compare with the results of Regner et al. and thin film measurements and find good qualitative agreement for both. Further experiments are suggested based on our predictions and the comparisons.

I. INTRODUCTION

The Allen and Feldman (AF) theory for disordered solids classifies vibrational modes in a disordered system as propagating (propagons, i.e. phonon-like), non-propagating (diffusons), and localized (locons).^{3,4} Several experimental measurements and estimates based on experiments demonstrate that propagating modes contribute significantly for amorphous silicon nitride² and amorphous silicon (a-Si),⁵⁻⁷ but not a-SiO₂.⁸⁻¹⁰ Using broadband frequency domain thermal-reflectance, Regner et al. measured how the thermal conductivity of a-SiO₂ and a-Si thin films change with the penetration depth associated with the heating laser pulse.¹ For a-SiO₂, the thermal conductivity of a 1000 nm film did not vary for penetration depths between 57 and 960 nm, suggesting that any propagating modes that contribute to thermal conductivity have MFPs below 57 nm. For a-Si, they find the thermal conductivities of thin films between 500 and 2000 nm vary by about 40% for penetration depths between 44 and 968 nm, suggesting that propagating modes with MFPs of 100 to 1000 nm contribute significantly to thermal conductivity.¹ Following the suggestion of Koh and Cahill, they interpret the measured value at a given penetration depth to be representative of the phonons with MFP less than that value, allowing for the construction of the so-called thermal conductivity accumulation function.¹¹⁻¹³

To understand the results of Regner et al. requires

knowledge of the MFPs of the propagating modes and the contribution from non-propagating modes. Experimentally, inelastic neutron scattering has been used to measure phonon lifetimes (MFPs) in materials, but this technique is more suited for single crystal samples.¹⁴ An x-ray diffraction and thermorefectance technique can measure ballistic transport in some structures, but is not well-suited for amorphous thin films.¹⁵ Traditionally, empirical expressions and simple models have been the only means to estimate MFPs in amorphous materials.¹⁶⁻²⁰ Because of this, the thermal conductivity accumulation function in amorphous materials is still not well understood.^{1,5-7,21-23}

Interpreting the measured thermal conductivity accumulation functions requires an understanding of how the MFPs of the low-frequency propagating modes scale with frequency.^{5-8,10,17,18,21,22} Experimental measurements of the thermal conductivity of thin films of a-SiO₂ and a-Si at varying temperatures gives indirect information about the low-frequency propagating modes.^{5-8,10,17,18,21,22,24,25} For a-SiO₂, varying temperature and film thickness^{8-10,17-20,26} measurements all suggest that the propagating modes contribute a negligible amount to thermal conductivity. However, the behavior of the low-frequency modes has only recently been understood by experimental measurements.^{10,27-30} For a-Si the low-frequency behavior of the MFPs is less understood.^{5-7,21-25} Temperature-varying²⁴ and film thickness-varying measurements^{5-7,21,22,24,31-37} suggest multiple different behavior of the low-frequency scaling

of the mean free paths of vibrational modes in a-Si.

The objective of this work is to investigate the propagating and non-propagating contributions to thermal conductivity of a-SiO₂ and a-Si by predicting the MFPs and thermal conductivity accumulation functions for realistic models to compare with recent measurements by Regner et al.¹ and experimental measurements for varying film thicknesses at 300 K.^{5–10,17–19,26,32} The paper is organized as follows. Using the Green-Kubo method and molecular dynamics (MD) simulations of large, realistic atomistic models of bulk a-SiO₂ and a-Si (including, to our knowledge, the largest MD simulation for a model of a-Si^{23,38}), we predict the total thermal conductivity in Section V A. Using MD simulations and lattice dynamics calculations, we predict the propagating and non-propagating mode diffusivities using a bottom-up approach based on the mode-by-mode properties in Section IV E and the total thermal conductivity in Section V A to compare with the GK method predictions. From the bottom-up approach, the spectrum of vibrational MFPs and the thermal conductivity accumulation functions are predicted for the first time for a-SiO₂ and a-Si in Section V B and compared with the measurements of Regner et al.¹ and experiments on thin films.^{5–10,17–19,26,32} Further experimentation is suggested based on the predictions from our models, previous experiments,^{5–10,17–19,26,32} and emerging broadband thermoreflectance techniques.^{1,12,13,39}

II. THEORETICAL FORMULATION OF VIBRATIONAL THERMAL CONDUCTIVITY

We calculate the total vibrational thermal conductivity, k_{vib} , of an amorphous solid from

$$k_{vib} = k_{pr} + k_{AF}, \quad (1)$$

where k_{pr} is the contribution from propagating (phonon-like) modes^{40–42} and k_{AF} is the contribution from diffusions (i.e., delocalized, non-propagating modes) predicted by the AF theory.²¹ Mode level properties obtained from MD simulations and lattice dynamics calculations will be used as inputs. The form of Eq. (1) has been used in previous studies of amorphous materials,^{5–8,10,17,18,21,22} all leading to predictions that while k_{pr} is a negligible fraction of k_{vib} for a-SiO₂ (< 10%),^{8,10} it is non-negligible for a-Si (> 20%).^{5–7,21–23}

The propagating contribution is modeled as^{21,22}

$$k_{pr} = \frac{1}{V} \int_0^{\omega_{cut}} DOS(\omega) C(\omega) D_{pr}(\omega) d\omega, \quad (2)$$

where V is the system volume, ω is the mode frequency, ω_{cut} is the maximum frequency of propagating modes, $DOS(\omega)$ is the vibrational density of states, $C(\omega)$ is the mode specific heat, and $D_{pr}(\omega)$ is the mode diffusivity. When using mode properties obtained from finite-sized

systems, it is more common to write Eq. (2) as a summation over the available modes. We choose the integral form because the required use of finite-sized simulation cells limit the lowest frequency modes that can be accessed and an extrapolation must be made to the zero frequency limit.^{5–8,10,21,22} Equation (2) is obtained by using the single-mode relaxation time approximation to solve the Boltzmann transport equation for a phonon gas.⁴² In the derivation of Eq. (2), the system is assumed to be isotropic (valid for an amorphous material) and have a single polarization,⁴¹ making the mode properties only a function of frequency. The choice of single polarization (i.e., an averaging of the transverse and longitudinal branches) does not significantly change the results predicted in this work or that of others.^{5–7,10,21,22} We will evaluate Eq. (2) under the Debye approximation, which assumes isotropic and linear dispersion such that the density of states is

$$DOS(\omega) = \frac{3\pi\omega^2}{2v_s^3}, \quad (3)$$

where v_s is an appropriate sound speed.⁴⁰

Because MD simulations are classical,⁴³ we take the specific heat to be k_B in the harmonic limit, where k_B is the Boltzmann constant. This harmonic approximation has been shown to be valid for a-Si modeled using the Stillinger-Weber (SW) potential at the temperature of interest here (300 K),²¹ and is generally valid for a range of systems such as Lennard-Jones (LJ) argon⁴⁴ and carbon nanotubes⁴⁵ for temperatures less than half the melting temperature. Taking the classical limit for the specific heat allows for a direct comparison between the MD- and lattice dynamics-based predictions. The full quantum expression for the specific heat is⁴²

$$C(\omega) = k_B \left[\frac{\hbar\omega/2k_B T}{\sinh(\hbar\omega/2k_B T)} \right]^2. \quad (4)$$

The quantum specific heat is used for the high-frequency diffusion modes predicted using lattice dynamics to compare our predictions for k_{AF} to experimental measurements in Sections V A and V B.

The diffusivity of the propagating modes is

$$D_{pr}(\omega) = \frac{1}{3} v_s^2 \tau(\omega), \quad (5)$$

where $\tau(\omega)$ is the frequency-dependent mode lifetime.⁴² An equivalent physical picture in terms of a scattering length is

$$D_{pr}(\omega) = \frac{1}{3} v_s \Lambda(\omega), \quad (6)$$

where $\Lambda(\omega)$ is the phonon mean free path (MFP), defined as

$$\Lambda(\omega) = v_s \tau(\omega). \quad (7)$$

The lifetimes will be modeled using

$$\tau(\omega) = B\omega^{-n}. \quad (8)$$

For amorphous materials, the scaling exponent n has been found experimentally and numerically to be between two and four,^{6,7,21–23,27–30,46–65} where a value of two corresponds to Umklapp scattering⁶⁶ and a value of four corresponds to Rayleigh scattering from point defects.⁶⁷ Combined with the form of the $DOS(\omega)$ [Eq. (3)], choosing $n \leq 2$ ensures that the thermal conductivity evaluated from Eq. (2) is finite. Choosing $n > 2$ causes the thermal conductivity to diverge, which can be fixed using additional anharmonic^{21,22} or boundary scattering terms.^{5–7}

The AF diffuson contribution to thermal conductivity is^{21,22}

$$k_{AF} = \frac{1}{V} \sum_{i, \omega_i > \omega_{cut}} C(\omega_i) D_{AF}(\omega_i), \quad (9)$$

where ω_i is the frequency of the i th diffuson mode, $C(\omega_i)$ is the diffuson specific heat, and $D_{AF}(\omega_i)$ is the diffuson diffusivity. Equation (9) is written as a sum because there are enough high-frequency diffusons in the finite-size systems studied here to ensure a converged value.^{21,22} The AF diffusivities are calculated from³

$$D_{AF}(\omega_i) = \frac{\pi V^2}{\hbar^2 \omega_i^2} \sum_{j \neq i} |S_{ij}|^2 \delta(\omega_i - \omega_j), \quad (10)$$

where \hbar the Planck constant and δ is the Dirac delta function. The heat current operator S_{ij} measures the thermal coupling between vibrational modes i and j based on their frequencies and spatial overlap of eigenvectors, can be calculated from harmonic lattice dynamics theory.^{3,21,22} For Eq. (10), S_{ij} is directionally averaged because the amorphous materials studied in this work are isotropic.

III. CALCULATION DETAILS

A. Sample Preparation

The three smallest a-SiO₂ samples are the same as those used in Ref. 68 and contain 288, 576, and 972 atoms at a density of 2350 kg/m³. These samples were prepared using a melt-quench procedure. Larger systems of 2880, 4608, and 34,562 atoms were created by tiling the smaller samples, melting at a temperature of 10,000 K and quenching instantaneously to 300 K at constant volume. A small sample of the resulting a-SiO₂ structure is shown in Fig. ?? (a). The 34,562 atom sample has a supercell side length of 8.052 nm. The atomic interactions are modeled using the modified Beest-Kramer-van Santen (BKS) potential^{69,70} from Ref. 68, except that the 24-6 LJ potential⁷¹ is changed to a 12-6, which has

a negligible effect on the predictions. The LJ potentials use a cutoff of 8.5 Å and the Buckingham potential uses a cutoff of 10 Å. The electrostatic interactions are handled using the Wolf direct summation method with a damping parameter of $\eta = 0.223 \text{ Å}^{-1}$ and a cutoff of 12 Å.⁷²

For a-Si, we use samples with 216, 1000, 4096, and 100,000 atoms generated from the modified Wooten-Winer-Weaire (WWW) algorithm from Ref. 38. A small sample of the a-Si structure is shown in Fig. ?? (b). Similar-sized samples of a-Si were studied in Ref. 23 using the MD-based direct method to predict thermal conductivity. A larger sample was created from the 100,000 atom sample by tiling it twice in all directions to create an 800,000 atom sample with a side length of 24.81 nm. All a-Si structures have a density of 2330 kg/m³, equivalent to the perfect crystal with a lattice constant of 5.43 Å. The SW potential is used to model the atomic interactions.⁷³

Amorphous materials may have many different atomic configurations with nearly equivalent potential energies leading to potential metastability during MD simulations.^{22,23,74–76} This meta-stability can cause errors when predicting vibrational lifetimes using Normal Mode Decomposition (NMD, see Section IV D). To remove metastability, all a-SiO₂ and a-Si samples were annealed at a temperature of 1100 K for 10 ns.^{22,23} The removal of meta-stability is demonstrated by a decrease and plateau of the sample's potential energy during the annealing.

B. Simulation Details

The MD simulations were performed using LAMMPS⁷⁸ with time steps of 0.905(a-SiO₂) and 0.5(a-Si) fs. Ten MD simulations with different initial conditions were run and the predictions from these simulations were ensemble averaged. All MD simulations are first equilibrated in an NVT (constant number of atoms, volume, and temperature) ensemble for 10^6 time steps. Data are then collected from simulations in the NVE (constant number of atoms, volume, and total energy) ensemble for 2^{21} time steps where the atomic trajectories are sampled every 2^8 time steps.

The Green-Kubo (GK) method is used to predict a top-down thermal conductivity k_{GK} [i.e., without using Eq. (1)].⁴³ using the first-avalanche method.⁷⁹ For system sizes of 4,608(a-SiO₂, supercell side length 4.026 nm) and 4,096(a-Si, supercell side length 4.344 nm) atoms, the trajectories from the MD simulations are also used with the NMD method to predict the vibrational mode lifetimes in Section IV D.

For an amorphous supercell the only allowed wave vector is the Gamma point (i.e., $\kappa = 0$), where κ is the wavevector and there are $3N_a$ polarization branches labeled by ν , where N_a is the number of atoms. Calculation of the vibrational modes at the Gamma point requires the eigenvalue solution of a dynamical matrix of size $(3N_a)^2$ that scales as $[(3N_a)^2]^3$, limiting the system sizes that can be considered to 4,608(a-SiO₂) and 4,096(a-Si) atoms. The eigenvalue solution is required to predict the vibrational DOS (Section IV A) and structure factors (Section IV B), and to perform the NMD calculations (Section IV D) and AF calculations (Section IV E). The frequencies and eigenvectors were computed using harmonic lattice dynamics calculations and GULP.⁸⁰ The calculation of the AF thermal diffusivities [Eq. (10)] is performed using GULP and a Lorentzian broadening of $14\delta\omega_{avg}$ for a-SiO₂ and $5\delta\omega_{avg}$ for a-Si, where $\delta\omega_{avg}$ is the average mode frequency spacing [$\delta\omega_{avg} = 1.8 \times 10^{10}$ (a-SiO₂) and 1.0×10^{10} (a-Si) rads/s].^{21,22} Varying the broadening by 10 % around these values does not change the resulting thermal conductivity k_{AF} significantly (see Section V A).

IV. VIBRATIONAL PROPERTIES

A. Density of States

The vibrational DOS is computed from

$$DOS(\omega) = \sum_i \delta(\omega_i - \omega), \quad (11)$$

where a unit step function of width $100\delta\omega_{avg}$ is used to broaden $\delta(\omega_i - \omega)$. The results for a-SiO₂ and a-Si are plotted in Fig. ?? The DOS for a-Si is similar to that of crystalline silicon,^{4,81} with peaks at mid- and high-frequencies. The DOS for a-SiO₂ is constant over most

of the frequency-range, with a gap that separates the high-frequency Si-O interactions.⁶⁸ There is a clear ω^{-2} scaling for both a-Si and a-SiO₂ at the lowest frequencies. The onset of this scaling occurs at a higher frequency for a-Si (between 1 to 2×10^{13} rads/s) than a-SiO₂ (between 4 to 5×10^{12} rads/s). This low-frequency scaling is predicted by the Debye model [Eq. (3)] and suggests that these modes may be propagating (i.e., phonon-like).

B. Structure Factor

Calculating the structure factors of the supercell Gamma modes is a method to test for their propagating (plane-wave) character at a particular wavevector and polarization. This approach has been previously used to predict effective dispersion curves of disordered and amorphous materials experimentally^{10,28,30,48,52,53,82–85} and numerically.^{4,21,22,49–51,54,56,59,60,64,86–91} The structure factor at a wavevector $\boldsymbol{\kappa}$ is defined as⁴

$$S^{L,T}(\boldsymbol{\kappa}) = \sum_{\nu} E^{L,T}(\boldsymbol{\kappa}_{\nu}) \delta(\omega - \omega(\boldsymbol{\kappa}_{\nu}^0)), \quad (12)$$

where the summation is over the Gamma modes, E^T refers to the transverse polarization and is defined as

$$E^L(\boldsymbol{\kappa}_{\nu}) = \left| \sum_b \hat{\boldsymbol{\kappa}} \cdot e(\boldsymbol{\kappa}_{\nu}^0 \frac{b}{\alpha}) \exp[i\boldsymbol{\kappa} \cdot \mathbf{r}_0(\frac{l=0}{b})] \right|^2 \quad (13)$$

and E^L refers to the longitudinal polarization and is defined as

$$E^T(\boldsymbol{\kappa}_{\nu}) = \left| \sum_b \hat{\boldsymbol{\kappa}} \times e(\boldsymbol{\kappa}_{\nu}^0 \frac{b}{\alpha}) \exp[i\boldsymbol{\kappa} \cdot \mathbf{r}_0(\frac{l=0}{b})] \right|^2. \quad (14)$$

In Eqs. (13) and (14), the b summations are over the atoms in the disordered supercell, $\mathbf{r}_0(\frac{l=0}{b})$ refers to the equilibrium atomic position of atom b , l labels the unit cells ($l = 0$ for the supercell), α labels the Cartesian coordinates, and $\hat{\boldsymbol{\kappa}}$ is a unit vector. The vibrational mode shape is contained in the $3N_a$ components of its eigenvector, $e(\boldsymbol{\kappa}_{\nu}^0 \frac{b}{\alpha})$.⁴¹

The transverse and longitudinal structure factors are plotted in Figs. ??(a) and ??(b) for a-SiO₂ and a-Si for wavevectors along the [100] direction of the supercells. Because amorphous structures are isotropic, the structure factors are direction-independent. Mode frequencies $[\omega_0(\boldsymbol{\kappa})]$ and linewidths $[\Gamma(\boldsymbol{\kappa})]$ can be predicted by fitting each structure factor peak $S^{L,T}(\boldsymbol{\kappa})$ to a Lorentzian function of the form

$$S^{L,T}(\boldsymbol{\kappa}) = \frac{C_0(\boldsymbol{\kappa})}{[\omega_0(\boldsymbol{\kappa}) - \omega]^2 + \Gamma^2(\boldsymbol{\kappa})}, \quad (15)$$

where $C_0(\nu)$ is a constant related to the DOS.⁸⁹ A dispersion relation is identified by plotting the $\omega_0(\boldsymbol{\kappa})$ values in the middle panels of Figs. ??(a) and ??(b), where the error bars indicate the linewidths. For a-Si, the Lorentzian fits to the structure factor peaks have coefficients of determination⁹² greater than 0.8 for $|\boldsymbol{\kappa}|/\kappa_{max} \leq 0.75$ and less than 0.7 for $|\boldsymbol{\kappa}|/\kappa_{max} > 0.75$. For a-SiO₂, the coefficients of determination are greater than 0.8 for $|\boldsymbol{\kappa}|/\kappa_{max} \leq 0.2$ and less than 0.7 for larger wavevector, where the structure factors peaks are less than an order of magnitude larger than the background.

For a-Si, the extracted dispersion is nearly linear at small wavevectors with a slight decrease in slope at the

largest values.^{21,22} For a-SiO₂, the dispersion is concave-down for the smallest wavevectors considered, transitioning to a strong concave-up dispersion at intermediate wavevectors. For the intermediate wavevectors, the longitudinal dispersion for a-SiO₂ is well-described by the so-called “dispersion law for diffusons”, where $\omega \propto \kappa^2$.⁸⁹ This large concave-up dispersion has been observed in experimental measurements and numerical models of amorphous materials^{10,49,54,56,83} including a-SiO₂.^{10,49,54,83} We note that at frequencies lower than 6.28×10^{11} rad/s, experimental measurements of a-SiO₂ recover a linear dispersion.^{10,28,30,53,83}

C. Group Velocity

For a disordered solid, except for the transverse and longitudinal sound speeds, there is not an accepted method to predict the group velocity of individual vibrational modes. While the structure factor gives the frequency spectrum needed to construct a propagating state with pure wavevector κ , the mode spectra $E^T(\kappa)$ and $E^L(\kappa)$ predict the plane-wave character of each mode.^{4,93} It is not generally possible to assign a unique wavevector to individual modes, even at low frequency,^{4,93} which makes predicting mode group velocities challenging. Attempts have been made to predict individual mode group velocities,^{23,81,94–97} but there is no theoretical basis for these proposed methods.

We now use the DOS and structure factors predicted in Sections IV A and IV B to predict the group velocity of the low-frequency modes for a-SiO₂ and a-Si. By fitting the DOS from Fig. ?? to Eq. (3), a sound speed is obtained and is reported in Table I. Because the DOS is a mixture of transverse and longitudinal modes, only a single sound speed can be predicted.

Both longitudinal and transverse sound speeds can be predicted from the structure factor peaks by finite differencing

$$v_s = \frac{\omega_0(d\kappa)}{d\kappa}. \quad (16)$$

Forward differencing is used on the lowest frequency peaks for a-SiO₂ and a-Si (Fig. ?? and the results are provided in Table I. The transverse and longitudinal sound speeds of a material can also be predicted from the material's bulk (G) and shear (K) moduli from

$$v_{s,T} = \frac{G^{1/2}}{\rho} \quad (17)$$

and

$$v_{s,L} = \frac{4G + 3K^{1/2}}{3\rho}. \quad (18)$$

Using the bulk and shear moduli defined in terms of the elastic constants according to the Voigt convention,⁸⁰ the corresponding sound speeds are reported in Table I.

The longitudinal and transverse sound speeds for a-SiO₂ predicted using the bulk and shear moduli are in reasonable agreement with predictions for a model with 8,016 atoms using the BKS potential (3,568 (transverse) and 5,937 (longitudinal) m/s).⁵⁴ Experimental measurements of the sound speeds using Brillouin light and inelastic x-ray scattering range between 3,800-4,000 (transverse) and 6,000-6,400 (longitudinal) m/s.^{46,48,53,83,98} Experimental measurements for quartz (c-SiO₂) are 3,700 (transverse) and 6,000 (longitudinal) m/s.^{99,100}

The transverse sound speeds predicted for a-Si are in good agreement with that predicted for a model created by a melt-quench procedure from MD simulation using the SW potential (3,600 (transverse)

m/s).¹⁰¹) A 1000 atom model using the SW potential and created by the original WWW algorithm predicted 3,670 (transverse) and 7,640 (longitudinal) m/s from the elastic constants,¹⁰² while a 4096 atom model predicted 7,590 (longitudinal) m/s from the structure factor.⁵⁶ A 4096 atom model created by the modified WWW algorithm³⁸ predicted 7,670 (longitudinal) m/s from the structure factor.⁵⁹ In an attempt to explain the anomalously high longitudinal sound speed (8,300 m/s) and thermal conductivity measurements in Ref. 6, three 1000 atom models relaxed using a tight-binding electron structure method predicted an average of 4,740 (transverse) and 7,830 (longitudinal) m/s.⁶ Experimental measurements using Rayleigh wave scattering are 3,420 and 4,290 (transverse) m/s for sputtered thin films and ion-bombarded a-Si, respectively.¹⁰³ Experimental measurements for c-Si show 4,810 (transverse) and 8,900 (longitudinal) m/s using Rayleigh wave scattering¹⁰³ and orientationally-averaged picosecond acoustics, respectively.⁷ Despite the variation in the experimental measurements and predictions from different models, the sound speed of a-Si is reduced compared to c-Si.

By annealing the structures (Section III A), the sound speeds predicted by the elastic moduli are increased. The sound speeds predicted by the elastic moduli for our models of a-SiO₂ and a-Si are less influenced by the finite size of our models than the structure factor and DOS values. The smaller values predicted by the structure factors and DOS results from the concave-down dispersion seen at low wavevector, particularly for a-SiO₂. The concave-down dispersion is less pronounced for a-Si, where the sound speeds predicted by all three methods are within five percent. By comparing the sound speeds in Table I, it is clear that the low-frequency DOS of our models for a-Si and a-SiO₂ are dominated by the transverse modes.

Under the Debye model (Eq. (3)), the *smaller* transverse sound speed makes the *larger* contribution to the DOS, which scales as the sound speed cubed. The intensity of the structure factors, which are directly proportional to the DOS,⁸⁹ was found to be four to five¹⁰⁴ and six to eight⁵⁴ times larger for transverse polarizations compared to longitudinal polarizations for models of a-SiO₂, which supports our finding that the DOS is dominated by transverse modes. The transverse sound speed predicted by the DOS, $v_{s,DOS}$, is used for both a-SiO₂ and a-Si throughout the rest of this work and is discussed in Section V A.

D. Lifetimes

We now predict the lifetimes of all vibrational modes in our models of a-SiO₂ and a-Si using the MD simulation-based NMD method,^{23,44,45,97,105–107} which explicitly includes the disorder in the supercell.^{23,90,95,96,108} In NMD,

TABLE I: Longitudinal and transverse sound speed estimated from the elastic moduli [Eqs. (18) and (17)], DOS [Eq. (3)], and structure factors [Eq. (16)]. The pre-annealed group velocities predicted by the elastic constants are $v_{s,T} = 3,670$, $v_{s,L} = 7,840$ m/s for a-Si and $v_{s,T} = 2,541$, $v_{s,L} = 4,761$ m/s for a-SiO₂ (see Section IV B).

method	moduli (m/s)	S^T, S^L (m/s)	DOS (m/s)
a-SiO ₂			
transverse	3,161	2,732	2,528
longitudinal	5,100	4,779	
a-Si			
transverse	3,886	3,699	3,615
longitudinal	8,271	8,047	

the atomic trajectories from an MD simulation are first mapped onto the vibrational mode coordinate time derivative,⁴¹

$$\dot{q}(\kappa=\mathbf{0}; t) = \sum_{\alpha, b, l}^{3, n, N} \sqrt{\frac{m_b}{N}} \dot{u}_\alpha(l; t) e^*(\kappa=\mathbf{0})_\alpha \exp[i(\mathbf{0} \cdot \mathbf{r}_0(l))]. \quad (19)$$

Here, m_b is the mass of the b_{th} atom in the supercell, \dot{u}_α is the α -component of the atomic velocity, and t is time. Because the supercells of a-SiO₂ and a-Si are disordered, the NMD method can only be performed at the Gamma point ($\kappa = \mathbf{0}$). The spectral energy of each vibrational mode, $\Phi(\nu, \omega)$, is calculated from

$$\Phi(\nu, \omega) = \lim_{\tau_0 \rightarrow \infty} \frac{1}{2\tau_0} \left| \frac{1}{\sqrt{2\pi}} \int_0^{\tau_0} \dot{q}(\kappa=\mathbf{0}; t) \exp(-i\omega t) dt \right|^2. \quad (20)$$

We choose the frequency-domain representation of the normal mode energy because we find it to be less sensitive to metastability of the amorphous structure than the time-domain representation.

The vibrational mode frequency and lifetime are predicted by fitting each mode's spectral energy to a Lorentzian function,

$$\Phi(\nu, \omega) = \frac{C_0(\nu)}{[\omega_0(\nu) - \omega]^2 + \Gamma^2(\nu)}, \quad (21)$$

where the constant $C_0(\nu)$ is related to the average energy of each mode and is valid when the linewidth $\Gamma(\nu) \ll \omega_0(\nu)$.⁴⁵ The mode lifetime is^{105,107}

$$\tau(\nu) = \frac{1}{2\Gamma(\nu)}. \quad (22)$$

The NMD-predicted lifetimes are plotted in Figs. ?? (a) and ?? (b) for a-SiO₂ and a-Si. Also plotted are the timescales extracted from the structure factor linewidths, $1/2\Gamma(\kappa)$ (Section IV B). For a-SiO₂, the NMD lifetimes are larger than the Ioffe-Regel (IR) limit $\tau = 2\pi/\omega$,⁴⁹ and are bounded by this limit at low frequencies. There

is no clear evidence for an ω^{-2} scaling, which would correspond to propagating modes. At mid-frequencies, the NMD lifetimes are approximately constant and there is a peak near 2×10^{14} rads/s, which corresponds to a peak in the DOS (see Fig. ??). The lifetimes predicted from the structure factor fall below the NMD-predicted lifetimes and the IR limit. These low values result because the structure factor for a-SiO₂ is evaluated for large wavevectors where the resulting wavepackets are formed by non-propagating modes.^{4,21,22}

For a-Si, the NMD lifetimes show a clear ω^{-2} scaling at low frequency. The lifetimes plateau at higher frequencies, over a wider range of frequencies than for a-SiO₂, with two peaks corresponding to peaks in the DOS (Fig. ??). A similar plateau of lifetimes at high frequencies has been reported for disordered lattices^{90,108,109} and other models of a-Si.²³ The transition from the low-frequency scaling to the plateau region occurs near 10^{13} rads/s, which corresponds to where the DOS peaks in Fig. ???. Similar behavior has been observed for models of disordered lattices.⁹⁰ The lifetimes predicted by the structure factor are in good agreement with those predicted by NMD at low frequencies. Similar agreement has been reported in other models of amorphous materials.^{22,110–112} The agreement between the NMD-predicted lifetimes and structure factor timescales for a-Si at low frequencies indicates that these modes are plane-wave like and the wavepackets formed by these modes are propagating.^{4,21,22}

The NMD-predicted lifetimes for a-Si range from 0.5 to 10 ps and are similar in magnitude to those predicted for previous models of a-Si.^{111–114} We note that one previous study of a-Si modeled using the Tersoff potential predicted vibrational lifetimes on the order of 100 ps, an order of magnitude larger than the values reported here and in previous studies.^{111–114} It is unclear what the source of this discrepancy is, although in Ref. 23 the NMD analysis was performed in the time domain where metastability can be more strongly pronounced. Using the Tersoff potential on the WWW a-Si models in this work, we predict similar lifetimes to the SW potential.

E. Diffusivities

Using the sound speeds predicted from the DOS (Table I), the NMD-predicted lifetimes for a-SiO₂ and a-Si are used to predict the mode diffusivities with Eq. (5) and are plotted in Figs. ?? (a) and ?? (b). We note that the sound speed is most appropriate for the lowest-frequency modes where the DOS scales as ω^2 (Fig. ??). To compare with the NMD predictions, the AF theory is also used to predict the mode diffusivities, which are also plotted in Figs. ?? (a) and ?? (b).

For a-SiO₂, the mode diffusivities predicted by NMD and AF agree well over the majority of the frequency range. The AF diffusivities at the highest frequencies show a sharp decrease, which is an indication that these modes are localized.²¹ The low- and mid-frequency diffusivities are above the high-scatter limit,

$$D_{HS} = \frac{1}{3} v_s a, \quad (23)$$

which assumes that all vibrational modes travel with the sound speed v_s and scatter over a distance of the lattice constant a .¹⁹

For a-SiO₂, the low frequency diffusivities do not show a definitive scaling. However, an ω^{-2} scaling can be fit to the AF theory predictions and the transition from propagating to non-propagating modes can be identified by choosing the cutoff frequency to be 4.55×10^{12} based on Ref. 10. This choice is discussed in Section V A. The constant B in Eq. (8) is fit to the AF-predicted diffusivities for frequencies below the cutoff.

For a-Si, the mode diffusivities predicted by NMD and AF at low frequencies show a clear ω^{-2} scaling. The NMD-predicted diffusivities are larger and show less scatter than those predicted by the AF theory, which is due to the finite-size system and the broadening that is required to evaluate Eq. (10).²¹ By using a larger broadening ($100\delta\omega_{avg}$), the scatter in the AF-predicted diffusivities at low frequency can be smoothed, but at the cost of decreasing the diffusivities at intermediate and high frequencies which affects the predicted diffuson contribution to thermal conductivity (see Section V A). It is possible that a frequency-dependent broadening may be necessary for a-Si and the AF theory, but determining this dependence is not necessary for interpreting our results. For a-Si the NMD- and AF-predicted diffusivities diverge near 10^{13} rads/s, while the NMD-predicted lifetimes are relatively constant above this frequency, indicating that the sound speed is no longer applicable. The AF diffusivities are larger than the high-scatter limit [Eq. (23)], except for the highest frequencies, which are localized.²¹

For a-Si, we choose ω_{cut} and B so that Eq. (5) is equal to the average AF-predicted diffusivity at the cutoff frequency. The resulting values are $\omega_{cut} = 1.1610^{13}$ rads/s and $B = 2.76 \times 10^{14} \text{ s}^{-1}$. This choice allows Eq. (5) to pass reasonably well through both the AF- and NMD-predicted diffusivities. For a-Si, we also consider a separate ω^{-4} scaling for Eq. (8) discussed in Section V A.

Because this scaling is not clear from the data in Fig. ?? (b), we use a cutoff frequency of 1.52×10^{13} rads/s from Refs. 21 and 5 and choose B so that Eq. (5) is equal to the average AF-predicted diffusivity at the cutoff frequency. We discuss these choices in Section V A.

While experiments show there is a cross-over region for the low-frequency diffusivity scaling of ω^{-2} to ω^{-4} ,^{27,30} the propagating contribution is still shown to be negligible for a-SiO₂.^{8,10} This cross-over region is observed for the frequency range of 4.6×10^9 to 1.52×10^{10} rads/s²⁷ and 3.04×10^{11} to 1.52×10^{12} rads/s³⁰. While this cross-over frequency can be identified experimentally for a-SiO₂,²⁷ experiments are limited for a-Si thin films.²⁵ Our present models are not large enough to investigate the mode-by-mode properties in this cross-over region.

Both a-SiO₂ and a-Si have a region at higher frequencies where the AF-predicted mode diffusivities are relatively constant. This behavior has been reported for model disordered systems such as disordered lattices^{89,90,109} and jammed systems.^{61,63} While diffusons are non-propagating modes whose MFPs are not well-defined,²¹ a diffuson MFP can be defined as

$$\Lambda_{AF}(\omega_i) = [3D_{AF}(\omega_i)\tau(\omega_i)]^{1/2}, \quad (24)$$

where $\tau(\omega_i)$ are the NMD-predicted lifetimes. Using this definition, $\Lambda_{AF}(\omega_i)$ for both a-SiO₂ and a-Si is found to vary between the lattice constant and the supercell size for modes with frequency above the cutoff. Similar MFPs have been estimated for diffusons in a-Si in previous studies.^{21,22} For modes with frequency below the cutoff, the MFPs range up to 4 (a-SiO₂) and 10 (a-Si) times the supercell side lengths. This result is in contrast to the MFPs estimated in Ref. 23 which ranged up to 100 times larger than the supercell side length. We believe that the origin of these large MFPs is a combination of their predicted lifetimes (see Section IV D) and the method used to estimate the mode group velocities.

V. THERMAL CONDUCTIVITY

A. Bulk

To predict the bulk thermal conductivity for our models of a-SiO₂ and a-Si, we use both Eq. (1) and the GK method. The GK method is computationally inexpensive compared to the NMD and AF methods so that larger system sizes can be accessed. The GK-predicted thermal conductivities for a-SiO₂ and a-Si are plotted in Fig. 1 versus the inverse of the system size. For a-SiO₂, there is no system-size dependence. The bulk thermal conductivity is estimated to be 2.1 ± 0.2 W/m-K by averaging over all the samples. This prediction is in agreement with the GK predictions in Ref. 68 within the uncertainties, but larger than the MD-based direct-method predictions in Ref. 115. The GK-predicted value in this work is larger than experimental measurements, which range between 1.3 and 1.5 W/m-K,^{1,9,19,26} because of the classical nature of the MD simulation (see Section II) and possibly the suitability of the BKS interatomic potential for modeling a-SiO₂.^{68,115} Quantum statistical effects are considered later in this section.

For a-Si, there is a clear system-size dependence. Because the low-frequency DOS has the form of Eq. (3) and the diffusivities scale as ω^{-2} , the thermal conductivity will scale as the inverse of the system size. The bulk value can be found by extrapolating to an infinite system size.^{45,116,117} The extrapolation is performed using the three largest system sizes, including the tiled 800,000 atom sample. We do not observe that tiling an a-Si model increases the thermal conductivity above the expected linear scaling as was found in Ref. 23 using the MD-based direct method. This finding is likely due to the small model used to perform the tiling in that study (512 atoms), while we use a large model (100,000 atoms). The extrapolated bulk value is 2.0 ± 0.2 W/m-K, which is less than that predicted in Ref. 23 using the Tersoff potential, where the uncertainty is estimated from the ensemble averaging for each system size. While it is difficult to create bulk a-Si experimentally,¹⁰³ our extrapolated bulk value is in reasonable agreement with experimental values for a wide range of thin film thicknesses (see Fig. 2).

To predict thermal conductivity from Eq. (1), we use the parameters B and ω_{cut} specified in Section IV E assuming an ω^{-2} scaling below ω_{cut} and the AF-predicted diffusivities. For a-SiO₂, the propagating, diffuson, and total thermal conductivities are 0.10 ± 0.05 , 1.9 ± 0.1 , and 2.0 ± 0.1 W/m-K (see Table II). The uncertainties are estimated by varying ω_{cut} by 10% and the AF broadening by 10%, respectively. The total value agrees with the GK value within the uncertainties. Baldi et al. estimated 0.1 W/m-K¹⁰ and Love and Anderson estimated 0.03 W/m-K⁸ for the propagating contribution using an expression similar to Eq. (2). Shenogin et al. predicted the total thermal conductivity of a-SiO₂ using non-equilibrium MD simulations of the same small structures used in this work, finding 2.0 W/m-K for their

largest system which was based on a 972 atoms model tiled in one direction six times.¹¹⁸ Their predicted diffuson conductivities are smaller than those in this work, which is due to a smaller broadening used for Eq. (10).

The transverse sound speed predicted for our model of a-SiO₂ is about 85% of that predicted by the other methods used here (Table I) and that measured by experiment.^{46,48,53,83,98} While using a smaller transverse sound speed leads to an underprediction of the mode diffusivity scaling [Eq. (5), Fig. ?? (a)], it leads to an overprediction of the DOS [Eq. (3)]. Holding all other input parameters in Eq. (1) constant, a smaller sound speed leads to a larger k_{pr} because the DOS scales as $1/v_s^3$. We can thus regard the prediction for k_{pr} from our model of a-SiO₂ as an upper bound. Our model confirms that propagating modes do not contribute significantly to the thermal conductivity of a-SiO₂.

By using the ω^{-2} diffusivity scaling for a-Si, the propagating, diffuson, and total thermal conductivity are 0.6 ± 0.2 , 1.2 ± 0.2 , and 1.8 ± 0.2 W/m-K. This value for total thermal conductivity is in agreement with the GK-predicted bulk value within the uncertainties. Earlier studies using similar models of a-Si to those used in this work find that k_{pr} is less than half of k_{vib} .^{21,22} A recent study of a-Si modeled using the Tersoff potential found $k_{ph} \approx k_{AF}$.²³ Estimates based on experimental measurements have shown k_{pr} as low as 20%^{5,22} and as high as 80% k_{vib} .^{6,7}

If an ω^{-4} scaling is assumed, the thermal conductivity diverges at low frequency. We bound the thermal conductivity by assuming the sample to be a thin film of thickness t_f and include the Matthiessen rule,¹¹⁹

$$\frac{1}{\tau_{eff}} = \frac{1}{\tau_{bulk}} + \frac{2v_s}{t_f}. \quad (25)$$

Using the largest film thickness from the experimental literature (80 μm)⁶ gives a propagating contribution to thermal conductivity of 3.0 ± 0.4 W/m-K, much larger than the GK-predicted bulk value. Using the ω^{-2} scaling and this film thickness gives a propagating contribution of 0.6 W/m-K (i.e., there is no effect). While predictions for k_{pr} for a-Si vary based on the assumed scaling of the low-frequency vibrational diffusivities^{5-7,21-23} all evidence supports that k_{pr} is a significant fraction of k_{vib} .^{1,5-7,21-23}

In Section II we approximated the specific heat of the propagating and non-propagating (diffuson) modes by the classical-limit value of k_B . For a temperature $T = 300$ K, the quantum heat capacity [Eq. (4)] at the largest cutoff frequency is $0.98k_B$, justifying the use of the classical specific heat in the propagating term in Eq. (2). For the AF contribution, however, the effect of quantum specific heat is important. At the highest frequencies in a-SiO₂ and a-Si, the specific heat is $0.073k_B$ and $0.47k_B$. Using Eq. (4) in Eq. (9) gives AF thermal conductivities of 1.4 ± 0.1 and 1.0 ± 0.1 W/m-K for a-SiO₂ and a-Si (Table II). This correction brings the estimate of k_{vib} for a-SiO₂ into good agreement with experimen-

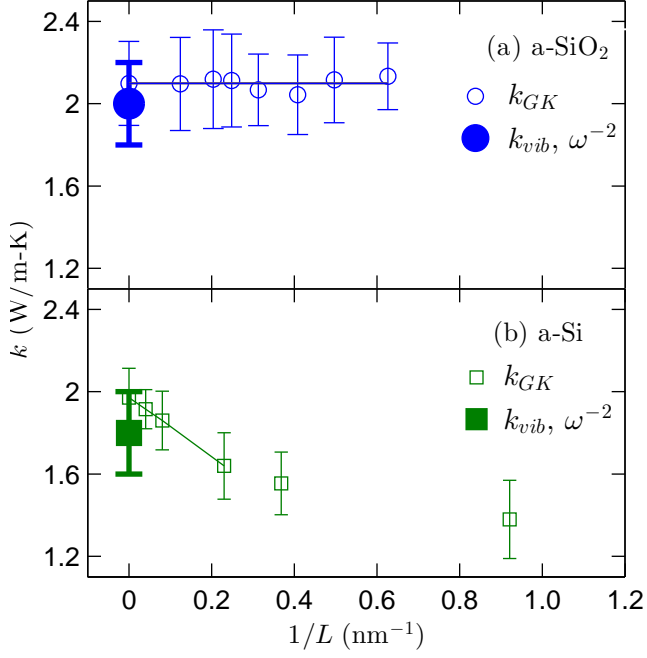


FIG. 1: Thermal conductivities of a-SiO₂ and a-Si predicted using the GK method and Eq. (1). For a-SiO₂, the GK-predicted thermal conductivity is size-independent, indicating that there is no important contribution from propagating modes. For a-Si, there is a clear size dependence, indicating the importance of propagating modes.

tal measurements.^{1,9,19,26} For a-Si, the modified k_{AF} is within 20 % of the classical-limit value, and does not significantly change the predicted k_{vib} . Because the change in k_{AF} due to quantum effects is small for a-Si, we keep the classical-limit value.

TABLE II: Total thermal conductivities for bulk a-SiO₂ and a-Si predicted by the GK method (k_{GK}) and Eq. (1) (k_{vib}). The total thermal conductivity k_{vib} is predicted from the propagating [k_{pr} , Eq. (2)] and non-propagating [k_{pr} , Eq. (9)] contributions. For the non-propagating contribution, classical and quantum specific heats are considered [Eq. (4)].

Conductivity (W/m-K)	a-SiO ₂	a-Si
k_{GK}	2.1 ± 0.2	2.0 ± 0.2
k_{vib}	2.0 ± 0.1	1.8 ± 0.2
k_{pr}	0.10 ± 0.05	0.6 ± 0.2
k_{AF} (classical)	1.9 ± 0.1	1.2 ± 0.1
k_{AF} (quantum)	1.4 ± 0.1	1.0 ± 0.1
k_{vib} (quantum)	1.5 ± 0.1	1.6 ± 0.2

B. Accumulation Function

The broadband frequency domain thermal-reflectance measurements by Regner et al.,¹ following the suggestion of Koh and Cahill,³⁹ interpret the measured thermal conductivity at a given penetration depth to be representative of the so-called thermal conductivity accumulation function.^{11,13} Their results are plotted in Fig. 2 (a) for a 1000 nm thick film of a-SiO₂ and in Fig. 2 (b) for 500 nm and 2000 nm thick films of a-Si. Based on the results in Section IV E, we will build thermal conductivity accumulation functions for a-SiO₂ and a-Si from

$$k(\Lambda_{max}) = k_{AF} + \frac{1}{V} \int_{\Lambda_{cut}}^{\Lambda_{max}} C(\Lambda) D(\Lambda) DOS(\Lambda) d\Lambda, \quad (26)$$

where Λ_{cut} is the MFP at the cut-off frequency, Λ_{max} is the maximum MFP considered in the thermal conductivity accumulation, and the propagating mode MFPs are calculated using Eq. (7). The diffuson contribution k_{AF} is evaluated using the quantum specific heat for a-SiO₂ (see Section V A). The results are plotted in Figs. 2 (a) and 2 (b), alongside available experimental measurements on thin films. For a-Si, the experimental measurements are grouped broadly by sample preparation technique: (A) chemical vapor deposition^{6,7,36} and (B) sputtered.^{5,34,35}

The predicted thermal conductivity accumulation function for a-SiO₂ saturates at a MFP of 10 nm, which is on the order of the finite size of our model. This result is in accord with the penetration depth-independent thermal conductivity measurements using broadband FDTR¹ and experimental measurements that show no film thickness dependence.^{9,26} For a-Si, the low-MFP plateau of thermal conductivity in the measurements of Regner et al. is consistent with our predicted k_{AF} . The propagating contribution to the accumulation is predicted using both ω^{-2} and ω^{-4} scalings. As discussed in Section V, the ω^{-2} scaling best describes the propagating contribution for our model of bulk a-Si. The thermal conductivity accumulation for the ω^{-2} scaling passes through the

largest penetration depth measurements of Regner et al., as well as some of the experimental measurements for varying film thicknesses.

We also consider the ω^{-4} scaling with the boundary scattering model [Eq. (25)] and an 80 μm thick film. The measurements of Regner et al. show much sharper accumulations than either the ω^{-2} or ω^{-4} scalings, particularly for a film of thickness 2 μm . Because of the large variation in experimental measurements, predictions for both ω^{-2} and ω^{-4} pass reasonably well through the experimental measurements of Regner et al. and on thin films. Amorphous silicon is typically prepared as thin films,¹⁰³ where voids and other inhomogeneities are unavoidable and can influence the vibrational structure at low frequencies.^{6,7,120–122} It is worth noting again that the results from thin film experiments have been interpreted using both ω^{-2} and ω^{-4} scalings.^{5–7,21,22}

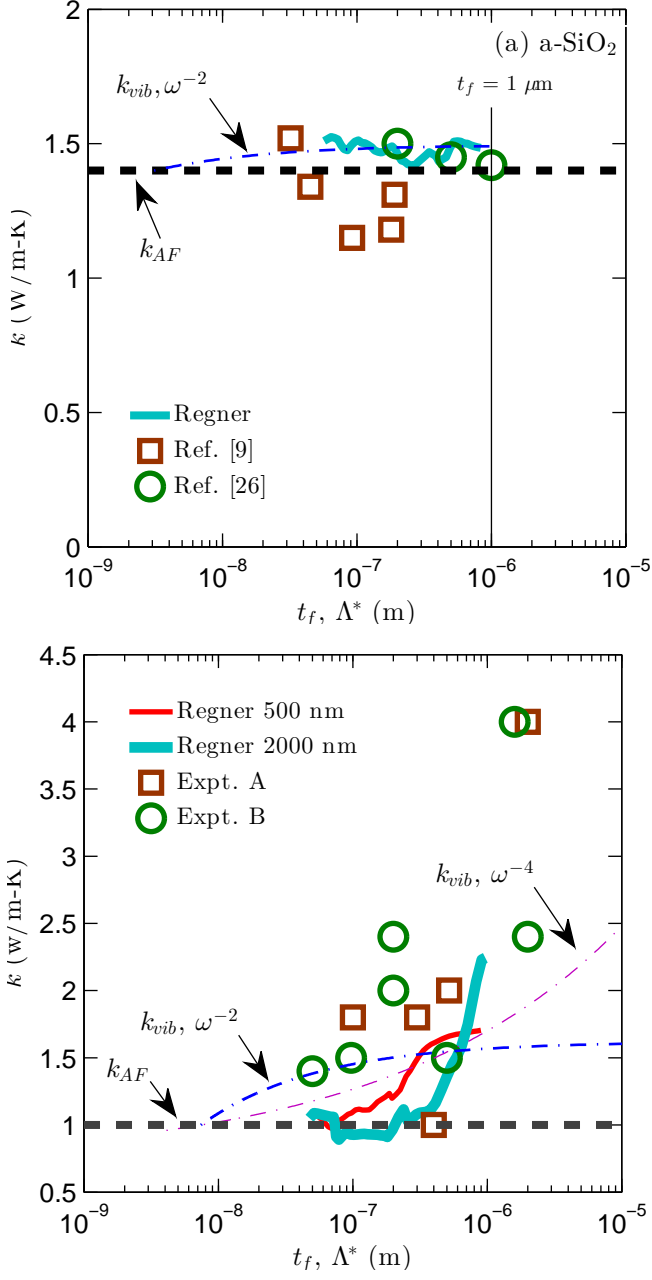


FIG. 2: (a) predicted thermal conductivity accumulation function [Eq. (26)] for a-SiO_2 compared with experimental measurements by Regner et al.,¹ Yamane et al. (Expt. A),²⁶ and Lee and Cahill (Expt. B).⁹ The predicted thermal conductivity accumulation demonstrates that the propagating contribution is negligible in our model, which is in accord with the experimental measurements. (b) predicted thermal conductivity accumulation function for a-Si compared with experimental measurements by Regner et al. and of sputtered (Expt. A),^{5,34,35} and chemical vapor deposited (Expt. B)^{6,7,33,36} thin films with a wide-range of film thicknesses. The predicted thermal conductivity accumulation demonstrates that the propagating contribution is significant for a-Si , while the agreement with the various experimental measurements is only qualitatively.

VI. SUMMARY

In this work we investigated the contributions of propagating (k_{ph}) and non-propagating (k_{AF}) modes to the total vibrational thermal conductivity k_{vib} of two amorphous materials, a-SiO₂ and a-Si, using the GK method (Section V A), NMD method (Section IV D), and AF theory (Section IV E). For our model of bulk a-Si, the thermal conductivity has significant contribution from propagating modes which are best described by a diffusivity scaling of ω^{-2} (see Section II). For a-SiO₂, the contribution from propagating modes was shown to be negligible (Section V A). This is confirmed by experimental thin film measurements^{8,10} and broadband frequency domain thermal reflectance measurements by Regner et al.¹

The thermal conductivity accumulation functions predicted for a-Si using both ω^{-2} and ω^{-4} scalings show reasonable agreement with the experimental measurements from Regner et al.¹ and on thin films.^{5-7,21,22} In fact, the existence of ω^{-2} and/or ω^{-4} scalings has been argued on the basis of the low-temperature (< 10 K) thermal conductivity plateau,^{18,21,22} which is observable in some preparations of a-SiO₂^{16,18-20} and a-Si^{6,31}, but absent in others.^{6,24,37}

The large discrepancies between measurements of a-

Si thin films suggest that a comprehensive experimental study using the recently developed broadband techniques^{1,12,39} on varying film thicknesses and preparation techniques is necessary. It may be particularly helpful to perform the experiments at temperatures less than < 10 K where the propagating contribution dominates for both a-SiO₂ and a-Si and the low-frequency scaling is still up for debate.^{5-8,10,18,19,21,22,32} Recent thermal conductivity measurements at room temperature of suspended amorphous silicon nitride bridges showed significant contributions from long MFP vibrations to heat transport,² which provides a comparison material to a-Si that deserves further investigation.

Acknowledgments

This work was supported by AFOSR award FA95501010098 and by a grant of computer time from the DOD High Performance Computing Modernization Program at the US Army Engineer Research and Development Center. We thank Davide Donadio, Joseph Feldman, Asad Hasan, Jonathan Malen, Craig Maloney, Normand Mousseau, Keith Regner, and Michael Widom for helpful discussions.

-
- ¹ K. T. Regner, D. P. Sellan, Z. Su, C. H. Amon, A. J. McGaughey, and J. A. Malen, *Nat Commun* **4**, 1640 (2013), URL <http://dx.doi.org/10.1038/ncomms2630>.
 - ² R. Sultan, A. D. Avery, J. M. Underwood, S. J. Mason, D. Bassett, and B. L. Zink, *Phys. Rev. B* **87**, 214305 (2013), URL <http://link.aps.org/doi/10.1103/PhysRevB.87.214305>.
 - ³ P. B. Allen and J. L. Feldman, *Physical Review B* **48**, 1258112588 (1993).
 - ⁴ P. B. Allen, J. L. Feldman, J. Fabian, and F. Wooten, *Philosophical Magazine B* **79**, 17151731 (1999).
 - ⁵ D. G. Cahill, M. Katiyar, and J. R. Abelson, *Physical Review B* **50**, 60776081 (1994).
 - ⁶ X. Liu, J. L. Feldman, D. G. Cahill, R. S. Crandall, N. Bernstein, D. M. Photiadis, M. J. Mehl, and D. A. Papaconstantopoulos, *Phys. Rev. Lett.* **102**, 035901 (2009), URL <http://link.aps.org/doi/10.1103/PhysRevLett.102.035901>.
 - ⁷ H.-S. Yang, D. G. Cahill, X. Liu, J. L. Feldman, R. S. Crandall, B. A. Sperling, and J. R. Abelson, *Phys. Rev. B* **81**, 104203 (2010), URL <http://link.aps.org/doi/10.1103/PhysRevB.81.104203>.
 - ⁸ M. S. Love and A. C. Anderson, *Phys. Rev. B* **42**, 18451847 (1990), URL <http://link.aps.org/doi/10.1103/PhysRevB.42.1845>.
 - ⁹ S.-M. Lee and D. G. Cahill, *Journal of Applied Physics* **81**, 25902595 (1997).
 - ¹⁰ G. Baldi, V. M. Giordano, G. Monaco, F. Sette, E. Fabiani, A. Fontana, and G. Ruocco, *Phys. Rev. B* **77**, 214309 (2008), URL <http://link.aps.org/doi/10.1103/PhysRevB.77.214309>.
 - ¹¹ C. Dames and G. Chen, in *Thermoelectrics Handbook: Macro to Nano*, edited by D. M. Rowe (Taylor & Francis, 2005), pp. 421–42–11.
 - ¹² A. J. Minnich, J. A. Johnson, A. J. Schmidt, K. Esfarjani, M. S. Dresselhaus, K. A. Nelson, and G. Chen, *Phys. Rev. Lett.* **107**, 095901 (2011), URL <http://link.aps.org/doi/10.1103/PhysRevLett.107.095901>.
 - ¹³ F. Yang and C. Dames, *Physical Review B* **87**, 035437 (2013), URL <http://link.aps.org/doi/10.1103/PhysRevB.87.035437>.
 - ¹⁴ A. D. Christianson, M. D. Lumsden, O. Delaire, M. B. Stone, D. L. Abernathy, M. A. McGuire, A. S. Sefat, R. Jin, B. C. Sales, D. Mandrus, et al., *Phys. Rev. Lett.* **101**, 157004 (2008), URL <http://link.aps.org/doi/10.1103/PhysRevLett.101.157004>.
 - ¹⁵ M. Highland, B. C. Gundrum, Y. K. Koh, R. S. Averback, D. G. Cahill, V. C. Elarde, J. J. Coleman, D. A. Walko, and E. C. Landahl, *Phys. Rev. B* **76**, 075337 (2007), URL <http://link.aps.org/doi/10.1103/PhysRevB.76.075337>.
 - ¹⁶ R. C. Zeller and R. O. Pohl, *Phys. Rev. B* **4**, 20292041 (1971), URL <http://link.aps.org/doi/10.1103/PhysRevB.4.2029>.
 - ¹⁷ J. E. Graebner, B. Golding, and L. C. Allen, *Phys. Rev. B* **34**, 56965701 (1986), URL <http://link.aps.org/doi/10.1103/PhysRevB.34.5696>.
 - ¹⁸ J. J. Freeman and A. C. Anderson, *Physical Review B* **34**, 5684 (1986).
 - ¹⁹ D. Cahill and R. Pohl, *Annual Review of Physical Chemistry* **39**, 93121 (1988).
 - ²⁰ D. G. Cahill and R. O. Pohl, *Solid State Communications* **70**, 927–930 (1989), ISSN 0038-

- 1098, URL <http://www.sciencedirect.com/science/article/pii/S038109889906303>.
- 21 J. L. Feldman, M. D. Kluge, P. B. Allen, and F. Wooten, *Physical Review B* **48**, 1258912602 (1993).
 - 22 J. L. Feldman, P. B. Allen, and S. R. Bickham, *Phys. Rev. B* **59**, 35513559 (1999), URL <http://link.aps.org/doi/10.1103/PhysRevB.59.3551>.
 - 23 Y. He, D. Donadio, and G. Galli, *Applied Physics Letters* **98**, 144101 (2011), URL <http://link.aip.org/link/APL/98/144101/1>.
 - 24 B. L. Zink, R. Pietri, and F. Hellman, *Physical Review Letters* **96**, 055902 (2006), URL <http://link.aps.org/doi/10.1103/PhysRevLett.96.055902>.
 - 25 D. B. Hondongwa, B. C. Daly, T. B. Norris, B. Yan, J. Yang, and S. Guha, *Phys. Rev. B* **83**, 121303 (2011), URL <http://link.aps.org/doi/10.1103/PhysRevB.83.121303>.
 - 26 T. Yamane, N. Nagai, S.-i. Katayama, and M. Todoki, *Journal of Applied Physics* **91**, 97729776 (2002), URL <http://link.aip.org/link/?JAP/91/9772/1>.
 - 27 C. Masciovecchio, G. Baldi, S. Caponi, L. Comez, S. Di Fonzo, D. Fioretto, A. Fontana, A. Gessini, S. C. Santucci, F. Sette, et al., *Phys. Rev. Lett.* **97**, 035501 (2006), URL <http://link.aps.org/doi/10.1103/PhysRevLett.97.035501>.
 - 28 G. Baldi, V. M. Giordano, G. Monaco, and B. Ruta, *Phys. Rev. Lett.* **104**, 195501 (2010), URL <http://link.aps.org/doi/10.1103/PhysRevLett.104.195501>.
 - 29 G. Baldi, V. M. Giordano, and G. Monaco, *Phys. Rev. B* **83**, 174203 (2011), URL <http://link.aps.org/doi/10.1103/PhysRevB.83.174203>.
 - 30 G. Baldi, M. Zanatta, E. Gilioli, V. Milman, K. Refson, B. Wehinger, B. Winkler, A. Fontana, and G. Monaco, *Phys. Rev. Lett.* **110**, 185503 (2013), URL <http://link.aps.org/doi/10.1103/PhysRevLett.110.185503>.
 - 31 G. Pompe and E. Hegenbarth, *physica status solidi (b)* **147**, 103 (1988), ISSN 1521-3951, URL <http://dx.doi.org/10.1002/pssb.2221470109>.
 - 32 D. G. Cahill, H. E. Fischer, T. Klitsner, E. T. Swartz, and R. O. Pohl, *Journal of Vacuum Science and Technology A* **7**, 12591266 (1989).
 - 33 L. Wiczorek, H. Goldsmid, and G. Paul, in *Thermal Conductivity 20*, edited by D. Hasselman and J. Thomas, J.R. (Springer US, 1989), pp. 235–241, ISBN 978-1-4612-8069-9, URL http://dx.doi.org/10.1007/978-1-4613-0761-7_22.
 - 34 B. S. W. Kuo, J. C. M. Li, and A. W. Schmid, *Applied Physics A: Materials Science & Processing* **55**, 289296 (1992), ISSN 0947-8396, 10.1007/BF00348399, URL <http://dx.doi.org/10.1007/BF00348399>.
 - 35 H. Wada and T. Kamijoh, *Japanese Journal of Applied Physics* **35**, L648L650 (1996), URL <http://jjap.jsap.jp/link?JJAP/35/L648/>.
 - 36 S. Moon, M. Hatano, M. Lee, and C. P. Grigoropoulos, *International Journal of Heat and Mass Transfer* **45**, 2439–2447 (2002), ISSN 0017-9310, URL <http://www.sciencedirect.com/science/article/pii/S0017931001003477>.
 - 37 B. L. Zink, R. Islam, D. J. Smith, and F. Hellman, *Phys. Rev. B* **74**, 205209 (2006), URL <http://link.aps.org/doi/10.1103/PhysRevB.74.205209>.
 - 38 G. T. Barkema and N. Mousseau, *Phys. Rev. B* **62**, 49854990 (2000), URL <http://link.aps.org/doi/10.1103/PhysRevB.62.4985>.
 - 39 Y. K. Koh and D. G. Cahill, *Phys. Rev. B* **76**, 075207 (2007), URL <http://link.aps.org/doi/10.1103/PhysRevB.76.075207>.
 - 40 N. W. Ashcroft and N. D. Mermin, *Solid State Physics* (Saunders, Fort Worth, 1976).
 - 41 M. T. Dove, *Introduction to Lattice Dynamics* (Cambridge, Cambridge, 1993).
 - 42 J. M. Ziman, *Electrons and Phonons* (Oxford, New York, 2001).
 - 43 D. A. McQuarrie, *Statistical Mechanics* (University Science Books, Sausalito, 2000).
 - 44 A. J. H. McGaughey and M. Kaviani, *Physical Review B* **69**, 094303 (2004).
 - 45 J. M. Larkin, J. E. Turney, A. D. Massicotte, C. H. Amon, and A. J. H. McGaughey, to appear in *Journal of Computational and Theoretical Nanoscience* (2012).
 - 46 R. Vacher, J. Pelous, F. Plicque, and A. Zarembowitch, *Journal of Non-Crystalline Solids* **45**, 397 (1981), ISSN 0022-3093, URL <http://www.sciencedirect.com/science/article/pii/S0022309381900600>.
 - 47 C. J. Morath and H. J. Maris, *Phys. Rev. B* **54**, 203213 (1996), URL <http://link.aps.org/doi/10.1103/PhysRevB.54.203>.
 - 48 P. Benassi, M. Krisch, C. Masciovecchio, V. Mazzacurati, G. Monaco, G. Ruocco, F. Sette, and R. Verbeni, *Phys. Rev. Lett.* **77**, 38353838 (1996), URL <http://link.aps.org/doi/10.1103/PhysRevLett.77.3835>.
 - 49 S. N. Taraskin and S. R. Elliott, *Philosophical Magazine Part B* **79**, 17471754 (1999), URL <http://www.tandfonline.com/doi/abs/10.1080/13642819908223057>.
 - 50 S. N. Taraskin and S. R. Elliott, *Phys. Rev. B* **61**, 1201712030 (2000), URL <http://link.aps.org/doi/10.1103/PhysRevB.61.12017>.
 - 51 W. Gtze and M. R. Mayr, *Phys. Rev. E* **61**, 587606 (2000), URL <http://link.aps.org/doi/10.1103/PhysRevE.61.587>.
 - 52 G. Ruocco, F. Sette, R. Di Leonardo, G. Monaco, M. Sampoli, T. Scopigno, and G. Viliani, *Phys. Rev. Lett.* **84**, 57885791 (2000), URL <http://link.aps.org/doi/10.1103/PhysRevLett.84.5788>.
 - 53 G. Ruocco and F. Sette, *Journal of Physics: Condensed Matter* **13**, 9141 (2001), URL <http://stacks.iop.org/0953-8984/13/i=41/a=307>.
 - 54 J. Horbach, W. Kob, and K. Binder, *The European Physical Journal B - Condensed Matter and Complex Systems* **19**, 531 (2001), ISSN 1434-6028, URL <http://dx.doi.org/10.1007/s100510170299>.
 - 55 A. Matic, D. Engberg, C. Masciovecchio, and L. Brjesson, *Phys. Rev. Lett.* **86**, 38033806 (2001), URL <http://link.aps.org/doi/10.1103/PhysRevLett.86.3803>.
 - 56 J. L. Feldman, *Journal of Non-Crystalline Solids* **307310**, 128 (2002), ISSN 0022-3093, URL <http://www.sciencedirect.com/science/article/pii/S0022309302014503>.
 - 57 B. Ruffl, M. Foret, E. Courtens, R. Vacher, and G. Monaco, *Phys. Rev. Lett.* **90**, 095502 (2003), URL <http://link.aps.org/doi/10.1103/PhysRevLett.90.095502>.
 - 58 W. Schirmacher, G. Ruocco, and T. Scopigno, *Phys. Rev. Lett.* **98**, 025501 (2007), URL <http://link.aps.org/doi/10.1103/PhysRevLett.98.025501>.
 - 59 J. K. Christie, S. N. Taraskin, and S. R. Elliott, *Journal of Non-Crystalline Solids* **353**, 2272 (2007),

- ISSN 0022-3093, URL <http://www.sciencedirect.com/science/article/pii/S0022309307002840>.
- ⁶⁰ H. Shintani and H. Tanaka, Nat Mater **7**, 870 (2008), ISSN 1476-1122, URL <http://dx.doi.org/10.1038/nmat2293>.
- ⁶¹ N. Xu, V. Vitelli, M. Wyart, A. J. Liu, and S. R. Nagel, Phys. Rev. Lett. **102**, 038001 (2009), URL <http://link.aps.org/doi/10.1103/PhysRevLett.102.038001>.
- ⁶² C. Ganter and W. Schirmacher, Phys. Rev. B **82**, 094205 (2010), URL <http://link.aps.org/doi/10.1103/PhysRevB.82.094205>.
- ⁶³ V. Vitelli, N. Xu, M. Wyart, A. J. Liu, and S. R. Nagel, Phys. Rev. E **81**, 021301 (2010), URL <http://link.aps.org/doi/10.1103/PhysRevE.81.021301>.
- ⁶⁴ M. Wyart, EPL (Europhysics Letters) **89**, 64001 (2010), URL <http://stacks.iop.org/0295-5075/89/i=6/a=64001>.
- ⁶⁵ S. Ayrinhac, M. Foret, A. Devos, B. Ruffl, E. Courtens, and R. Vacher, Phys. Rev. B **83**, 014204 (2011), URL <http://link.aps.org/doi/10.1103/PhysRevB.83.014204>.
- ⁶⁶ J. Callaway, Physical Review **113**, 1046 (1959).
- ⁶⁷ P. G. Klemens, Proceedings of the Physical Society. Section A **68** (1955).
- ⁶⁸ A. J. H. McGaughey and M. Kaviani, International Journal of Heat and Mass Transfer **47**, 17831798 (2004).
- ⁶⁹ B. W. H. van Beest, G. J. Kramer, and R. A. van Santen, Physical Review Letters **64**, 19551958 (1990).
- ⁷⁰ G. J. Kramer, N. P. Farragher, B. W. H. van Beest, and R. A. van Santen, Physical Review B **43**, 50685080 (1991).
- ⁷¹ Y. Guissani and B. Guillot, The Journal of Chemical Physics **104**, 7633 (1996), URL <http://link.aip.org/link/?JCP/104/7633/1>.
- ⁷² D. Wolf, P. Keblinski, S. R. Phillpot, and J. Eggebrecht, The Journal of Chemical Physics **110**, 8254 (1999), URL <http://link.aip.org/link/?JCP/110/8254/1>.
- ⁷³ F. H. Stillinger and T. A. Weber, Physical Review B **31**, 52625271 (1985).
- ⁷⁴ U. Buchenau, H. M. Zhou, N. Nucker, K. S. Gilroy, and W. A. Phillips, Phys. Rev. Lett. **60**, 13181321 (1988), URL <http://link.aps.org/doi/10.1103/PhysRevLett.60.1318>.
- ⁷⁵ M. Durandurdu and D. A. Drabold, Phys. Rev. B **66**, 155205 (2002), URL <http://link.aps.org/doi/10.1103/PhysRevB.66.155205>.
- ⁷⁶ N. Bernstein, J. L. Feldman, and M. Fornari, Phys. Rev. B **74**, 205202 (2006), URL <http://link.aps.org/doi/10.1103/PhysRevB.74.205202>.
- ⁷⁷ K. Momma and F. Izumi, Journal of Applied Crystallography **41**, 653658 (2008), URL <http://dx.doi.org/10.1107/S0021889808012016>.
- ⁷⁸ S. Plimpton, Journal of Computational Physics **117**, 1 19 (1995), ISSN 0021-9991, URL <http://www.sciencedirect.com/science/article/pii/S002199918571039X>.
- ⁷⁹ J. Chen, G. Zhang, and B. Li, Physics Letters A **374**, 23922396 (2010), ISSN 0375-9601, URL <http://www.sciencedirect.com/science/article/pii/S0375960110004081>.
- ⁸⁰ J. D. Gale and A. L. Rohl, Molecular Simulation **29**, 291 (2003).
- ⁸¹ D. Donadio and G. Galli, Phys. Rev. Lett. **102**, 195901 (2009).
- ⁸² F. Sette, M. H. Krisch, C. Masciovecchio, G. Ruocco, and G. Monaco, Science **280**, 1550 (1998), URL <http://www.sciencemag.org/content/280/5369/1550.abstract>.
- ⁸³ B. Ruzicka, T. Scopigno, S. Caponi, A. Fontana, O. Pilla, P. Giura, G. Monaco, E. Pontecorvo, G. Ruocco, and F. Sette, Phys. Rev. B **69**, 100201 (2004), URL <http://link.aps.org/doi/10.1103/PhysRevB.69.100201>.
- ⁸⁴ D. Kaya, N. L. Green, C. E. Maloney, and M. F. Islam, Science **329**, 656 (2010), URL <http://www.sciencemag.org/content/329/5992/656.abstract>.
- ⁸⁵ N. L. Green, D. Kaya, C. E. Maloney, and M. F. Islam, Physical Review E **83**, 051404 (2011), URL <http://link.aps.org/doi/10.1103/PhysRevE.83.051404>.
- ⁸⁶ S. Volz and G. Chen, Physical Review B **61**, 26512656 (2000).
- ⁸⁷ V. Martin-Mayor, M. Mezard, G. Parisi, and P. Verrocchio, The Journal of Chemical Physics **114**, 8068 (2001), URL <http://link.aip.org/link/?JCP/114/8068/1>.
- ⁸⁸ S. Ciliberti, T. S. Grigera, V. Martin-Mayor, G. Parisi, and P. Verrocchio, The Journal of Chemical Physics **119**, 8577 (2003), URL <http://link.aip.org/link/?JCP/119/8577/1>.
- ⁸⁹ Y. M. Beltukov, V. I. Kozub, and D. A. Parshin, Phys. Rev. B **87**, 134203 (2013), URL <http://link.aps.org/doi/10.1103/PhysRevB.87.134203>.
- ⁹⁰ J. Larkin and A. McGaughey, Journal of Applied Physics (2013).
- ⁹¹ A. Marruzzo, W. Schirmacher, A. Fratalocchi, and G. Ruocco, Sci. Rep. **3** (2013), URL <http://dx.doi.org/10.1038/srep01407>.
- ⁹² J. Cowpe, J. Astin, R. Pilkington, and A. Hill, A collection of papers presented at the Euro Mediterranean Symposium on Laser Induced Breakdown Spectroscopy (EMSLIBS 2007) **63**, 1066 (2008), ISSN 0584-8547, URL <http://www.sciencedirect.com/science/article/pii/S0584854708002656>.
- ⁹³ R. Biswas, A. M. Bouchard, W. A. Kamitakahara, G. S. Grest, and C. M. Soukoulis, Phys. Rev. Lett. **60**, 22802283 (1988), URL <http://link.aps.org/doi/10.1103/PhysRevLett.60.2280>.
- ⁹⁴ J. C. Duda, T. S. English, D. A. Jordan, P. M. Norris, and W. A. Soffa, Journal of Physics: Condensed Matter **23**, 205401 (2011), URL <http://stacks.iop.org/0953-8984/23/i=20/a=205401>.
- ⁹⁵ Y. He, D. Donadio, J.-H. Lee, J. C. Grossman, and G. Galli, ACS Nano **5**, 18391844 (2011), URL <http://pubs.acs.org/doi/abs/10.1021/nn2003184>.
- ⁹⁶ Y. He, D. Donadio, and G. Galli, Nano Letters **11**, 3608\textbackslashtextbackslashashtextbackslashtextbackslashashtextbackslashtextbackslashashtextbackslash963611 (2011).
- ⁹⁷ T. Hori, T. Shiga, and J. Shiomi, Journal of Applied Physics **113**, 203514 (2013), URL <http://link.aip.org/link/?JAP/113/203514/1>.
- ⁹⁸ A. Polian, D. Vo-Thanh, and P. Richet, EPL (Europhysics Letters) **57**, 375 (2002), URL

- doi/10.1103/PhysRevB.43.2152.
- ¹⁰³ R. Vacher, H. Sussner, and M. Schmidt, Solid State Communications **34**, 279 (1980), ISSN 0038-1098, URL <http://www.sciencedirect.com/science/article/pii/0038109880905578>.
 - ¹⁰⁴ S. N. Taraskin and S. R. Elliott, EPL (Europhysics Letters) **39**, 37 (1997), URL <http://stacks.iop.org/0295-5075/39/i=1/a=037>.
 - ¹⁰⁵ A. J. C. Ladd, B. Moran, and W. G. Hoover, Physical Review B **34**, 50585064 (1986).
 - ¹⁰⁶ A. S. Henry and G. Chen, Journal of Computational and Theoretical Nanoscience **5**, 112 (2008).
 - ¹⁰⁷ J. E. Turney, E. S. Landry, A. J. H. McGaughey, and C. H. Amon, Phys. Rev. B **79**, 064301 (2009), URL <http://link.aps.org/doi/10.1103/PhysRevB.79.064301>.
 - ¹⁰⁸ Y. He, I. Savic, D. Donadio, and G. Galli, Phys. Chem. Chem. Phys. p. (2012), URL <http://dx.doi.org/10.1039/C2CP42394D>.
 - ¹⁰⁹ P. Sheng and M. Zhou, Science **253**, 539542 (1991), URL <http://www.sciencemag.org/content/253/5019/539.abstract>.
 - ¹¹⁰ V. Mazzacurati, G. Ruocco, and M. Sampoli, EPL (Europhysics Letters) **34**, 681 (1996), URL <http://stacks.iop.org/0295-5075/34/i=9/a=681>.
 - ¹¹¹ S. R. Bickham and J. L. Feldman, Phys. Rev. B **57**, 1223412238 (1998), URL <http://link.aps.org/doi/10.1103/PhysRevB.57.12234>.
 - ¹¹² S. R. Bickham, Phys. Rev. B **59**, 48944897 (1999), URL <http://link.aps.org/doi/10.1103/PhysRevB.59.4894>.
 - ¹¹³ J. Fabian and P. B. Allen, Phys. Rev. Lett. **77**, 38393842 (1996), URL <http://link.aps.org/doi/10.1103/PhysRevLett.77.3839>.
 - ¹¹⁴ J. Fabian, J. L. Feldman, C. S. Hellberg, and S. M. Nakhmanson, Phys. Rev. B **67**, 224302 (2003), URL <http://link.aps.org/doi/10.1103/PhysRevB.67.224302>.
 - ¹¹⁵ P. Jund and R. Jullien, Physical Review B **59**, 1370713711 (1999).
 - ¹¹⁶ J. Shiomi, K. Esfarjani, and G. Chen, Physical Review B **84**, 125209 (2011).
 - ¹¹⁷ K. Esfarjani, G. Chen, and H. T. Stokes, Physical Review B **84**, 085204 (2011).
 - ¹¹⁸ S. Shenogin, A. Bodapati, P. Keblinski, and A. J. H. McGaughey, Journal of Applied Physics **105**, 034906 (2009), URL <http://link.aip.org/link/?JAP/105/034906/1>.
 - ¹¹⁹ D. P. Sellan, J. E. Turney, A. J. H. McGaughey, and C. H. Amon, Journal of Applied Physics **108**, 113524 (2010).
 - ¹²⁰ J. L. Feldman, N. Bernstein, D. A. Papaconstantopoulos, and M. J. Mehl, Phys. Rev. B **70**, 165201 (2004), URL <http://link.aps.org/doi/10.1103/PhysRevB.70.165201>.
 - ¹²¹ S. Li, Y. Jiang, Z. Wu, J. Wu, Z. Ying, Z. Wang, W. Li, and G. J. Salamo, Applied Surface Science **257**, 8326 (2011), ISSN 0169-4332, URL <http://www.sciencedirect.com/science/article/pii/S0169433211004715>.
 - ¹²² S. Li, Y. Jiang, Z. Wu, J. Wu, Z. Ying, Z. Wang, W. Li, and G. Salamo, Journal of Materials Science: Materials in Electronics **23**, 224 (2012), ISSN 0957-4522, URL <http://dx.doi.org/10.1007/s10854-011-0390-1>.